NAWCWPNS TM 8069

Transfer Alignment

by
Sherryl H. Stovall
Navigation and Data Link Section
Systems Engineering Division

DECEMBER 1996

NAVAL AIR WARFARE CENTER WEAPONS DIVISION
China Lake , CA 93555-6001

FOREWORD

This report defines various types of transfer alignment and describes software developed to model these transfer alignment mechanizations using both simulated data and real engineering data recorded on a United Kingdom Defense Research Agency test aircraft.

Work on this project was supported in part by Naval Air Warfare Center Weapons Division (NAWCWPNS) discretionary funding and was performed in 1995 and 1996. The aircraft data was supplied via a loan agreement between the U.S. and the U.K.

The original software described in this report was coded by Dr. Robert Rogers. Additional algorithms were coded by Mr. David Brough. Mr. Rene Lemonnier managed the many details of the loan agreement.

L. GILBERT, Head
Systems Engineering Division
17 December 1996

NAWCWPNS TM 8069, published by Code 471120D, 24 copies.

TECHNICAL MEMORANDUM (TM)
BIBLIOGRAPHIC INFORMATION

REPORT NUMBER	REPORT DATE	DISTRIBUTION STATEMENT
NAWCWPNS TM 8069	December 1996	Statement D; critical technology

REPORT TITLE

Transfer Alignment

AUTHOR(S) *(Name, code, and telephone number)*	NUMBER OF COPIES	NUMBER OF PAGES
Sherryl H. Stovall, Code 471120D	24	35

ABSTRACT *(Maximum 200 words)*

(U) This report defines various types of transfer alignment and describes software developed to model these transfer alignment mechanizations using both simulated data and real engineering data.

SECURITY CLASSIFICATION OF REPORT	SECURITY CLASSIFICATION OF ABSTRACT	SECURITY CLASSIFICATION OF THIS PAGE
UNCLASSIFIED	UNCLASSIFIED	UNCLASSIFIED

NAWCWPNS 3900/1 (11-92)

CONTENTS

Introduction 3

Transfer Alignment 3

Simulation 5

Test Data 7

Data Analysis 8
- Simulated Data 8
- Real Data 14

Summary 19

Appendix: Measurement Equations 21

References 35

Figures:
1. Transfer Alignment Simulation, Simulated Data Mode 6
2. Transfer Alignment Simulation, Real Data Mode 7
3. Single Runs for Each Type of Accelerometer-Based Alignment 10
4. Single Runs for Each Type of Accelerometer-Based Alignment With Increased Vibration Levels 11
5. Angular Rate 12
6. Integrated Angular Rate 13
7. Double Integrated Angular Rate 14
8. Horizontal Velocity Error Versus Time (Straight and Level Flight) 15
9. Velocity Error Versus Time (60-Degree Turn) 16
10. Velocity Error Versus Time With Gyro-Based Measurements Added 17
11. Delta Pitch 18
12. Delta Roll 19

Tables:

1. One-Sigma Tilt Errors at End of Alignment 8
2. One-Sigma Velocity Errors at End of Drift 8
3. Position Errors at End of Drift 8
4. Linear Displacement 9
5. Angular Displacement 9
6. Linear Displacement (Increased Vibration Levels) 10
7. Angular Displacement (Increased Vibration Levels) 10

INTRODUCTION

Any inertial navigation system (INS) requires initialization. This initialization may take many forms, the simplest being a one-time transfer of position, velocity, and attitude data. For most applications, this initialization must be refined by some alignment process. In a generic alignment, the INS processes measurements from some external reference to improve its navigation solution. In this report we are concerned with a particular type of alignment, called a transfer alignment, in which the external reference is another INS. Several types of transfer alignment are described in the report. The transfer alignment process has been modeled in a computer simulation, which was used to analyze the various types of alignment. The analysis was based on both real and simulated data. We present a quantitative and qualitative comparison of the various transfer alignment mechanizations and try to indicate under what circumstances a particular method is applicable. We also give a brief description of the computer simulation that has been created to perform the general analysis and that may be used to perform an analysis for a particular application of the methods described below.

TRANSFER ALIGNMENT

In the describing the transfer alignment process we refer to the reference INS as the master and to the INS being aligned as the slave. Alignments are based on measurements. In the measurement process, the slave creates an estimate of some quantity based on its navigation solution. The same quantity is computed based on the master's reported navigation solution. The difference in these two quantities is then filtered to obtain estimates of the errors in the slave's navigation solution and in some cases its sensor errors. The transfer alignment process assumes that the master's navigation solution is perfect; thus, the accuracy of the alignment is limited by the degree to which this assumption is valid. The type of filter almost universally used in this application is a Kalman filter, which computes gains based on its current estimate of all the statistical errors modeled in the system. These gains multiply the measurement to produce corrections to the various error states modeled in the filter. The filter then updates its estimate of the system errors (covariance matrix) to reflect these corrections. The covariance is propagated forward in time (via the State Transition Matrix, based on the differential equations for the system error states) until the next measurement becomes available.

In general, the slave is displaced from the master. This displacement, referred to as a moment arm, must be accounted for in constructing measurements. The slave's sensor axes may also be rotated from those of the master. Hence, all measurements must be referred to a common reference frame. It is usually assumed, to first order, that the master and slave are part of a rigid body. Deviations from this rigid body assumption are modeled as moment arm flexure and linear and angular vibration. These disturbances will be modeled as measurement noise and process noise in the filter (accurate modeling of these quantities will require adding extra states to the filter). We identify two distinct types of transfer alignment, those based on measurements derived from accelerations (accelerometer-based alignments) and those from rotations (gyro-based alignments).

Accelerometer-based alignments are of three types:
1. Velocity matching
2. Integrated velocity (position) matching
3. Doubly integrated velocity matching

Gyro-based alignments are of three types:
1. Angular rate matching
2. Integrated angular rate (angle) matching
3. Doubly integrated angular rate matching

Equations for implementing these measurements are given in the Appendix.

A few general remarks are in order at this point. For a navigation system error or a sensor error to be observable, the error mode must be "excited." This merely means that the error produces some measureable output that is a function of the system error states. For example, an error in determining the vertical will result in horizontal velocity errors, because the gravity vector will be resolved in the wrong frame (we are concerned here only with near-Earth navigators). If the "tilt" error is some small angle θ, the acceleration error will be approximately $g \sin \theta$ where g is the magnitude of the gravitational acceleration. This illustrates a significant difference between the two types of alignments. In an accelerometer-based alignment, gravity excites the horizontal tilt errors and, through the filtering process, lets us observe errors such as gyro bias errors that result in time-dependent tilt errors. Therefore, the alignment process continues during straight and level flight. This is also the reason that some maneuvering such as a horizontal turn or a longitudinal acceleration is required to make heading errors and vertical gyro bias errors observable.

In contrast, in a gyro-based alignment mechanization, the only observable errors during straight and level flight are gyro bias errors. These types of alignments require turns about all three axes in order to excite the system error modes and are best used in conjunction with some programmed aircraft maneuver. Some investigators have reported good results in processing these types of measurements at high rates (References 1 through

3). It should be noted that these measurements are useful only for correcting attitude and gyro bias errors. Gyro-based alignments will not correct velocity errors or accelerometer errors. Neither type of alignment will correct position errors.

Some maneuvering is also beneficial to the alignment process because it allows us to decorrelate errors. The classic example of this concerns the correlation of tilt errors and accelerometer bias errors. The filter cannot distinguish between these two error states during straight and level flight and therefore apportions any horizontal acceleration error between these states based on its *a priori* estimate of these errors. The filter will thus reach a steady-state solution, and no further corrections will be applied to these states. The residual errors will in effect cancel and make no contribution to the horizontal velocity errors during straight and level flight. During a turn, these states will be decorrelated in the filter, which allows further estimation of these errors.

If all measurements were noise free, the three accelerometer-based alignments would all be equivalent. Theoretically, they would all produce identical alignments for a given scenario. The main advantage of the higher-order alignments lies in their ability to suppress measurement noise. An integration is equivalent to a first-order low-pass filter. Each additional integration is equivalent to adding an additional pole to the filter. This decreased effective measurement noise results in a more accurate alignment, all other conditions being equal. Another way of stating this is that for a given disturbance noise, the higher-order alignments require less maneuvering to allow the filter to estimate a given navigation or sensor error. This phenomenon is discussed in more detail in References 4 and 5. Note, however, that the disturbance noise does not just disappear. For example, a disturbance that appears as measurement noise in a velocity matching alignment would be represented as process noise in an integrated velocity matching alignment. The increased noise filtering is gained at the cost of an increase in algorithm complexity and filter state size, so the type of alignment should be chosen to fit the requirements of a particular application. Analysis does indicate that the integrated velocity matching alignment, for example, (References 6 and 7) is more robust in the presence of modeling errors than the velocity matching alignment. Similar remarks apply to gyro-based alignments.

SIMULATION

The analysis described in this report was performed on software developed by the Navigation and Data Link Section of the Naval Air Warfare Center Weapons Division (NAWCWPNS). The transfer alignment simulation executes in two distinct modes. In the Simulated Data Mode (Figure 1), the input data is generated in software. The trajectory generator is a path segment generator that is set up to approximate the desired flight path. From the output of the trajectory generator, we develop $\Delta\theta's$ and $\Delta\upsilon's$ as an input to the

slave navigator. These inputs are corrupted with sensor error models and additive noise. The noise may be white noise, random walk, and first- or second-order Markov noise. These simulated gyro and accelerometer outputs are used by the slave navigation model to generate a navigation solution. The slave navigation channel is duplicated by a master navigator model, which generates its own independent navigation solution. The master navigator outputs can be replaced by truth data. The master and slave outputs are then used to construct a measurement (one of the six listed above). Noise is added to the measurement, which is then processed by a Kalman filter. The output of the filter is used to correct the slave navigation and sensor errors. This mode is useful for theoretical analysis, as we control the input errors and we also know the "truth" from the trajectory generator. This mode is also useful for debugging software. The simulation can be used as a Monte Carlo simulation with the input errors randomly generated based on user-defined statistical models. Statistics are computed for the ensemble of runs.

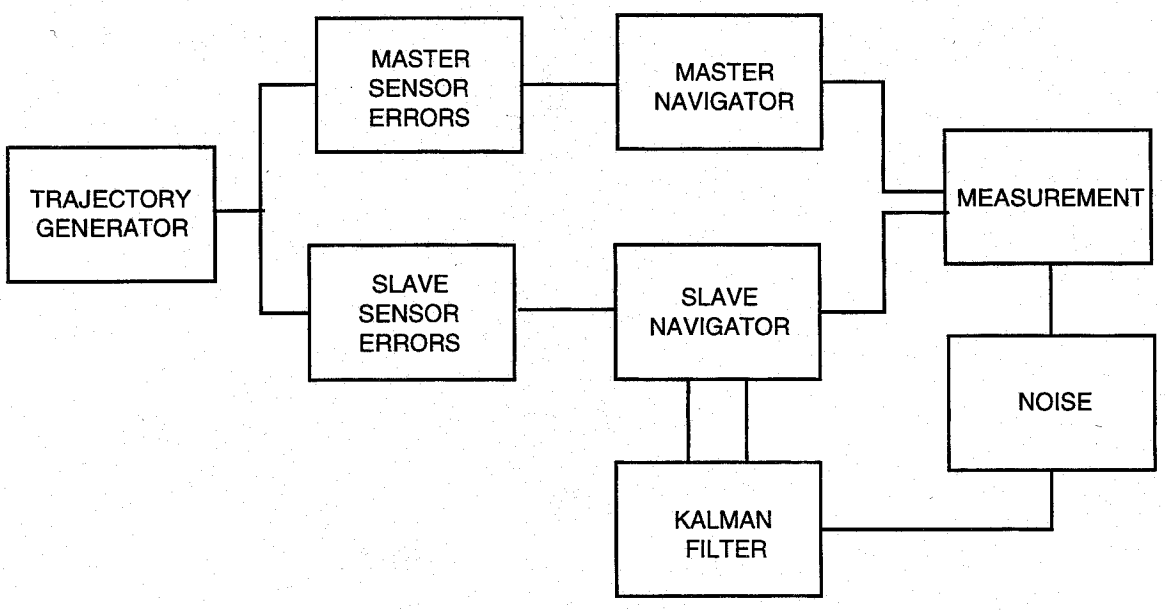

FIGURE 1. Transfer Alignment Simulation, Simulated Data Mode.

In the Real Data Mode (Figure 2), we use navigation data recorded from a reference INS and $\Delta\theta's$ and $\Delta\upsilon's$ recorded from a test INS. The data is processed as described above, except that we do not normally add sensor errors and noise in this mode. We also perform only one run at a time because we do not control the input errors. The use of real engineering data provides a means of validating both the software and the measurement models. It also provides a tool for analysis of flight data.

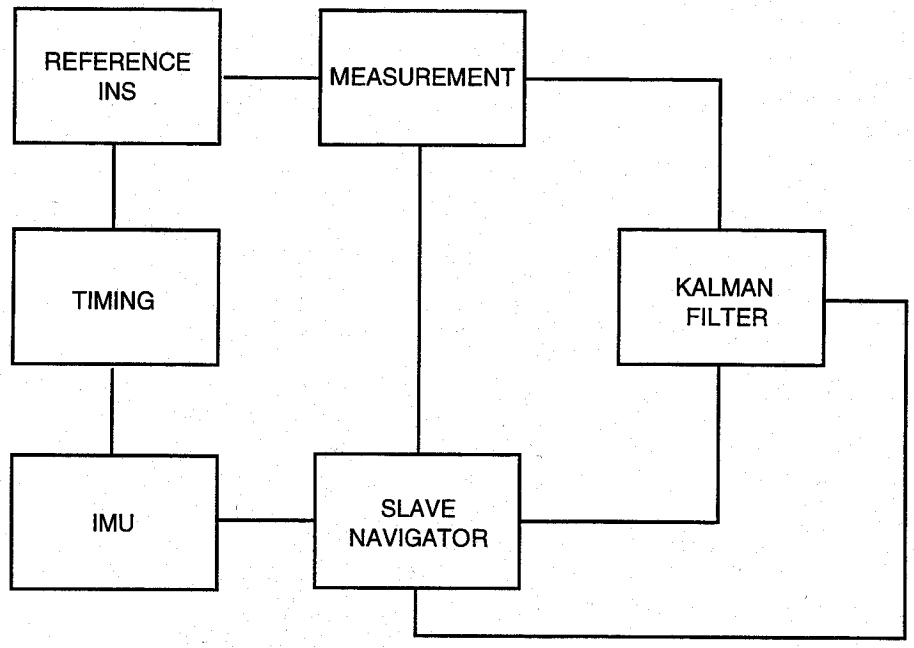

FIGURE 2. Transfer Alignment Simulation, Real Data Mode.

TEST DATA

The engineering data used in preparing this report was supplied by the British Defence Research Agency (DRA) under a Memorandum of Understanding (MOU) with NAWCWPNS. The data was collected with instrumentation installed on a DRA Tornado aircraft. Two test flights were flown in the U.K. in January 1996. These flights resulted in approximately 2 hours and 20 minutes of test data. The instrumentation consisted of equipment installed in a modified fuel tank carried under the fuselage of the aircraft and a modified 1000-pound bomb casing installed on the wing pylon. The fuel tank contained the reference INS (Litton LN93), a Data Acquisition Unit, a clock, and a dual 486 P.C. to act as a controller. The bomb casing contained a Kearfott T-16 Inertial Measurement Unit supplied by NAWCWPNS under the MOU. The data consisted of time-tagged position, velocity, and attitude data from the reference INS and time-tagged $\Delta\theta's$ and $\Delta\upsilon's$ from the T-16. Data was recorded at 51.2 Hz. Software was written to time-synchronize the data and convert it to files compatible with the transfer alignment simulation.

DATA ANALYSIS

SIMULATED DATA

We begin with simulated data, because we can control all of the input parameters in this mode. We also know the "truth" in this case, which allows us to compute absolute errors rather than relative errors. Because single runs are merely indicators and carry little statistical significance, a set of Monte Carlo runs was performed for velocity matching and integrated velocity matching alignments. Each set of runs consisted of 50 alignments following identical profiles. These were a minimal type alignment limited to two 30-degree, half-*g* turns during the alignment phase. The duration of the alignment was 360 seconds. A position and velocity reset were performed at the end of the alignment. A 2-*g*, 60-degree turn was executed after the alignment was completed. Total navigation time was 290 seconds. The parameters defining the vibration and flexure were based on measured values for a representative air-to-ground missile. Tables 1 through 3 list some of the results of these runs for both types of alignment.

TABLE 1. One-Sigma Tilt Errors at End of Alignment.

Tilt errors, deg	Velocity match	Velocity integral
Pitch	0.0241	0.0158
Roll	0.0234	0.0113
Heading	0.0579	0.0325

TABLE 2. One-Sigma Velocity Errors at End of Drift.

Velocity error, ft/s	Velocity match	Velocity integral
North	5.70	5.00
East	5.41	4.16
Down	0.28	0.18

TABLE 3. Position Errors at End of Drift.

Position error, ft	Velocity match	Velocity integral
Vertical	82.2	54.6
Horizontal	905.0	693.0

The integrated velocity matching alignments produce more accurate alignments than velocity matching even for the relatively low noise levels modeled here. These noise levels, modeled as second-order Markov processes, are defined in Tables 4 and 5. The noise parameters are defined in the Appendix.

TABLE 4. Linear Displacement.

Axis	N, ft^2/s^3	α	β, s^{-1}	σ_v, ft/s	σ_x, in.	ω, Hz
x	0.375	0.40	20.1	0.105	0.063	2.93
y	0.146	0.17	24.8	0.093	0.045	3.89
z	0.389	0.40	23.1	0.103	0.053	3.37

TABLE 5. Angular Displacement.

Axis	N, deg^2/s^3	α	β, s^{-1}	σ_ω, rad/s	σ_θ, deg	ω, Hz
x	101.8	0.15	25.8	0.045	0.100	4.05
y	18.0	0.15	49.8	0.014	0.016	7.75
z	8.3	0.18	26.8	0.011	0.024	4.19

The doubly integrated velocity matching alignments were not run in the Monte Carlo mode because the version of the transfer alignment simulation that contains the higher-order alignment modes has not yet been configured for Monte Carlo runs.

To make the above results more concrete, we present the results of single runs for each type of accelerometer-based alignment (Figure 3). The flight profile and noise parameters are the same as in the Monte Carlo runs described above. The runs were identical except for the alignment mode. The results of the integrated velocity matching and the doubly integrated velocity matching alignments are indistinguishable at this noise level.

To exhibit more clearly the effects of noise, we repeat the above with the increased vibration levels defined in Tables 6 and 7 (Figure 4). In this case we see an improvement with the increased filtering provide by the higher-order alignments.

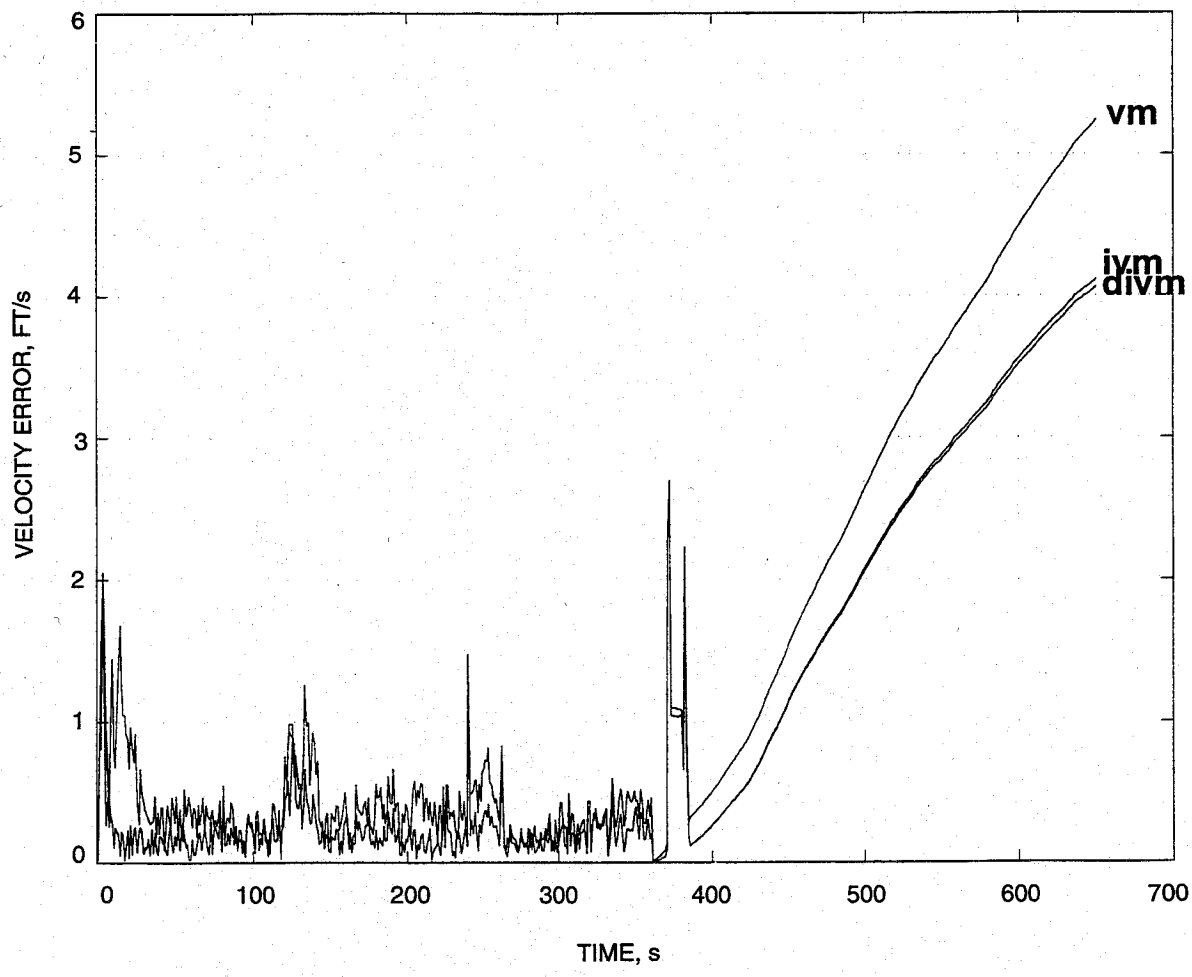

FIGURE 3. Single Runs for Each Type of Accelerometer-Based Alignment.

TABLE 6. Linear Displacement (Increased Vibration Levels).

Axis	N, ft^2/s^3	α	β, s^{-1}	σ_v, ft/s	σ_x, in.	ω, Hz
x	50.0	0.40	12.5	1.58	1.52	1.82
y	50.0	0.17	12.5	2.43	2.33	1.96
z	50.0	0.40	23.1	1.16	0.60	3.37

TABLE 7. Angular Displacement (Increased Vibration Levels).

Axis	N, deg^2/s^3	α	β, s^{-1}	σ_ω,rad/s	σ_θ, deg	ω, Hz
x	1.0E3	0.15	25.8	0.140	0.311	4.05
y	1.0E4	0.15	49.8	0.319	0.367	7.75
z	1.0E4	0.18	26.8	0.397	0.849	4.19

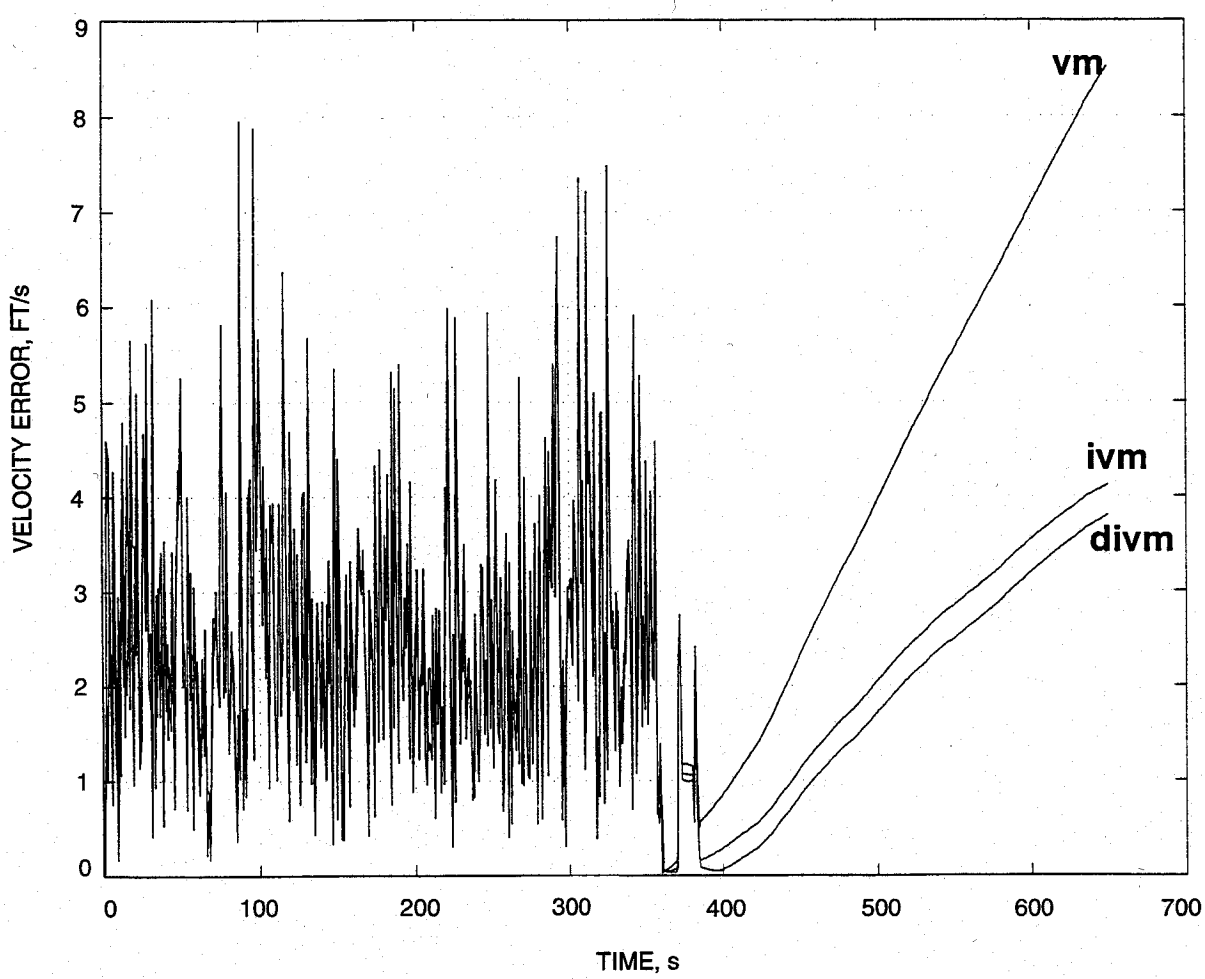

FIGURE 4. Single Runs for Each Type of Accelerometer-Based Alignment With Increased Vibration Levels.

Because gyro-based alignments require turning maneuvers in order to estimate errors, a special flight profile was created to exhibit these types of alignments (Figures 5 through 7). The 20-second alignment phase consists of an 18-degree pitch-up-then-down, followed by a 45-degree, 5-*g* turn and two 60-degree rolls. These maneuvers are followed by a short 10-second navigation as we are interested only in attitude alignment in this case. The initial tilt and heading errors were 1 degree per axis. Measurements were taken at a 10-Hz rate. The angular noise is given in Table 5.

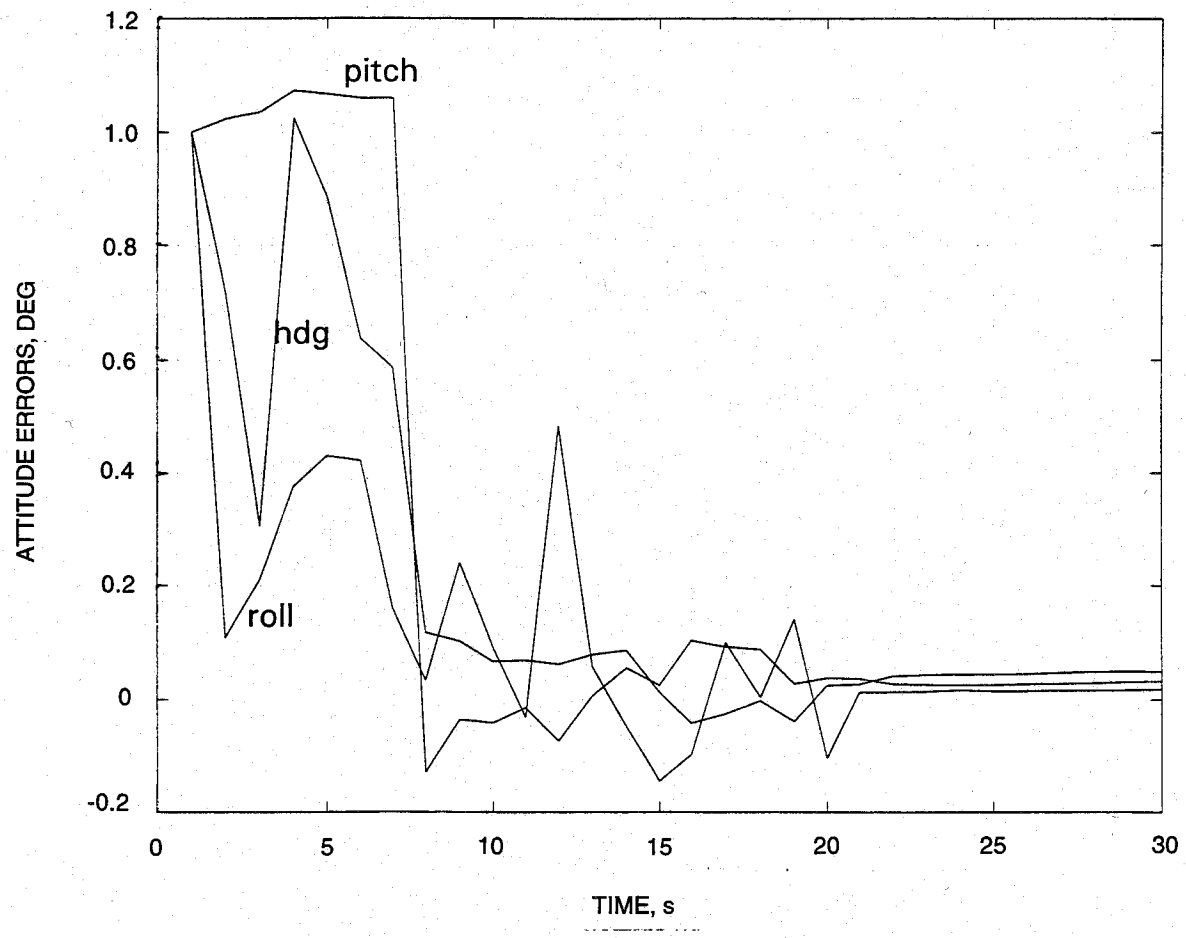

FIGURE 5. Angular Rate.

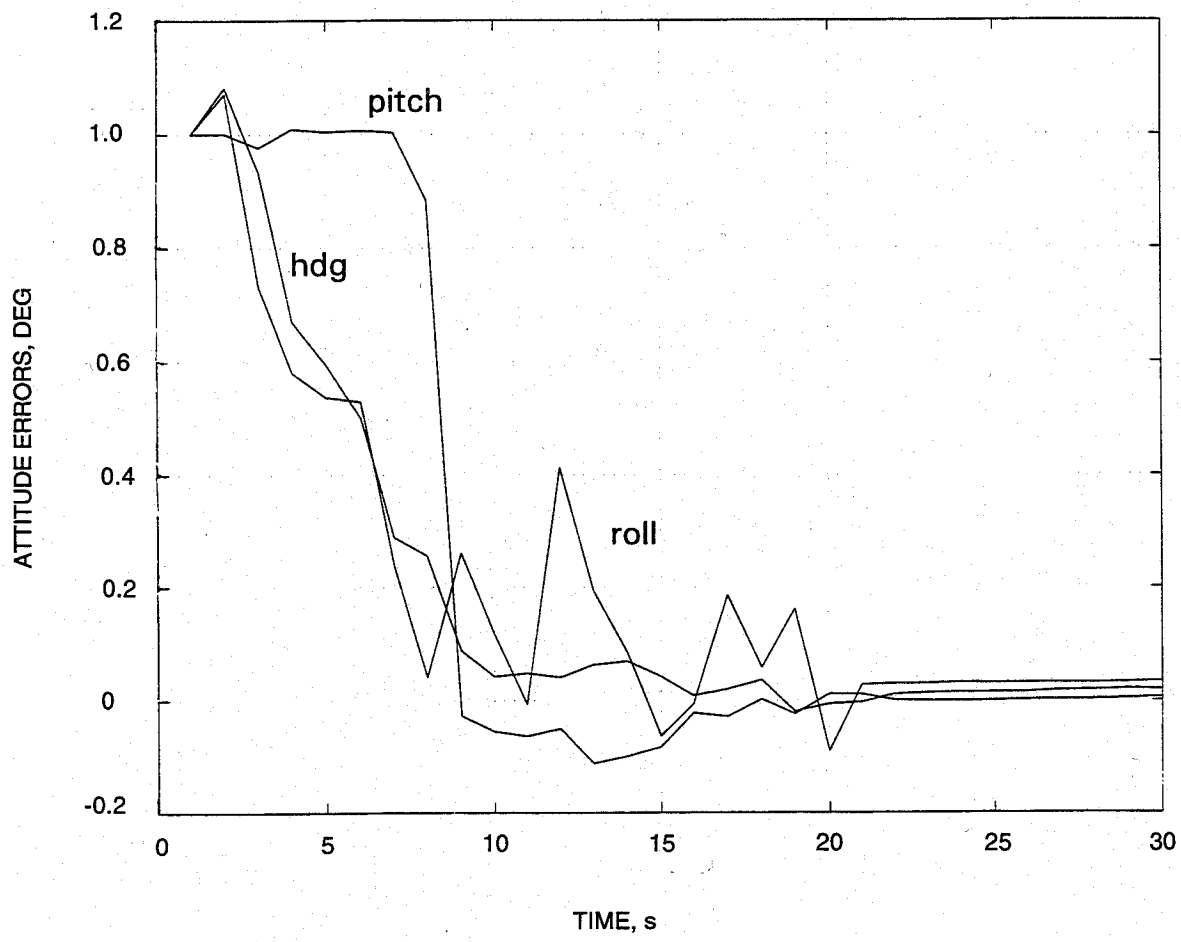

FIGURE 6. Integrated Angular Rate.

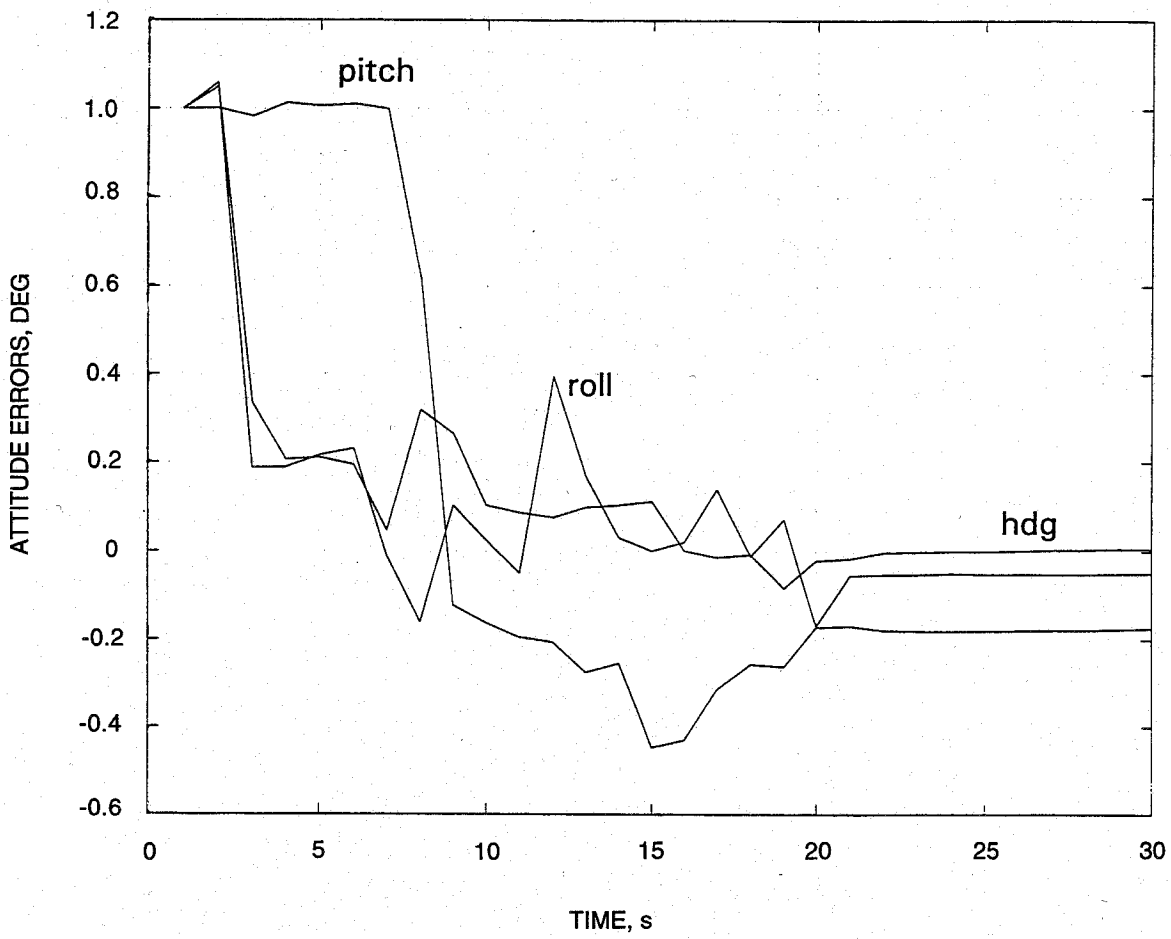

FIGURE 7. Doubly Integrated Angular Rate.

The doubly integrated angular rate alignments showed a 3-milliradian bias on the pitch axis. This problem has not yet been explained. None of the gyro-based alignment methods could perform an alignment with the vibration levels specified in Table 7.

REAL DATA

The validation of both the simulation and the alignment algorithms is provided by the demonstrated ability to process real data. In this section we present some results of alignments performed using the data obtained from the U.K. Data was collected from two flights in January 1996. The analysis in this section was performed using a flight segment of approximately 21 minutes in duration, consisting of 390 seconds of straight and level

flight followed by a slow 60-degree turn. Next a series of four ±30-degree turns was performed. These were coordinated turns of 1.5, 2.0, 3.0, and 4.0 *g*. These turns were followed by a slow 180-degree turn. The rest of the segment is straight and level flight.

Figure 8 shows the horizontal velocity error versus time for the three accelerometer-based alignment mechanizations. These alignments are all 360 seconds in duration and occur during the initial straight and level portion of the flight. The excursions in velocity error during the turns are caused by heading error. In the case of the velocity matching alignment this is quite pronounced for the 180-degree turn at 43,600 seconds. The doubly integrated velocity matching alignment shows no significant improvement over the integrated velocity matching alignment in this case.

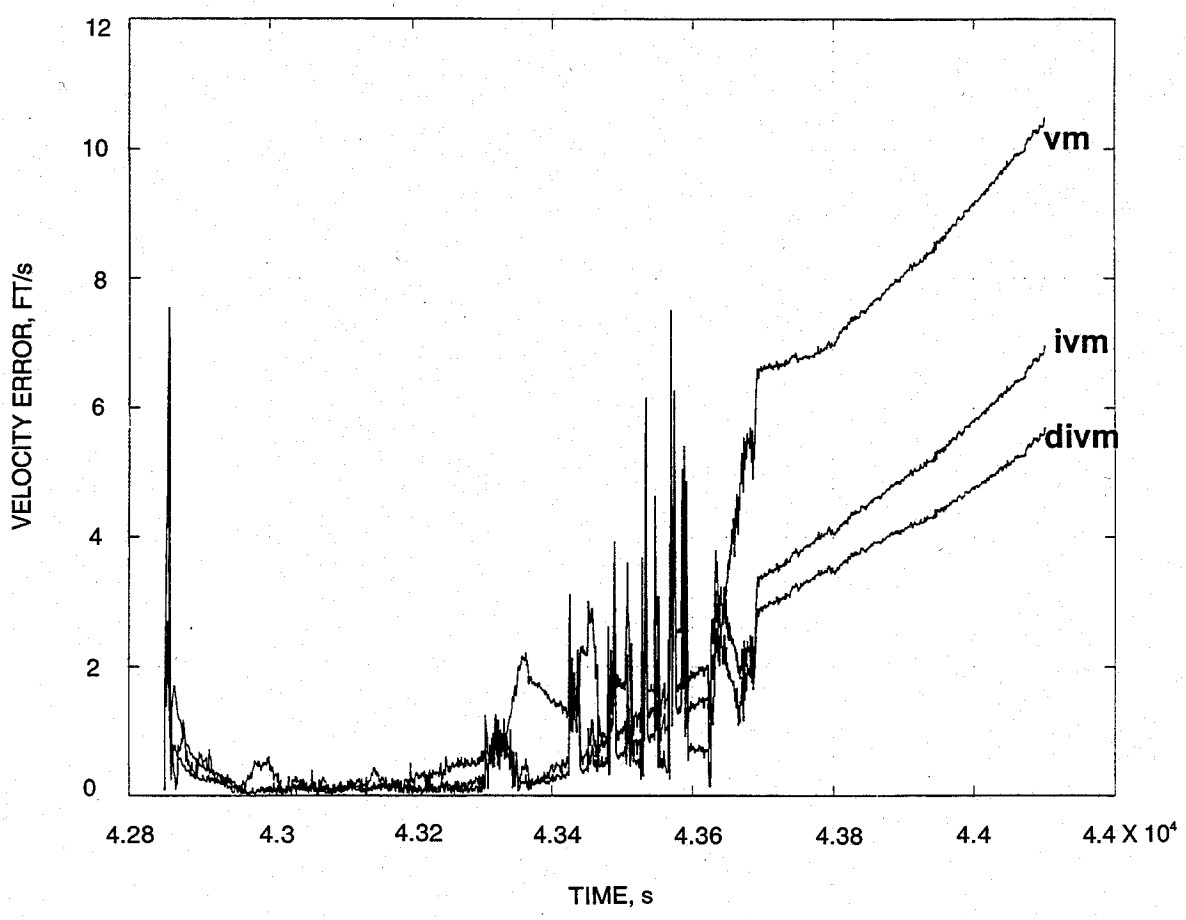

FIGURE 8. Horizontal Velocity Error Versus Time (Straight and Level Flight).

The large spikes in the data are caused by two things. First, the error is defined as the difference between the test IMU's navigation solution and the reference data. The horizontal velocity error is derived from the x- and y-axis velocities of the slave and master. Because these velocities are in slightly different frames, there is some apparent difference as the system rotates. Second, there is some small unresolved time difference in the data logging between the slave and master.

In the next plot (Figure 9), we extend the alignment to include the 60-degree turn at 43,300 seconds. We note that the excursions during the turns are less in this plot than in Figure 8 but that the error slopes are larger for the velocity matching and integrated velocity matching cases. These differences indicate that the three alignments did a better job inestimating heading (which is what we expect when we include turns) but a poorer job in estimating tilts, probably because the alignments ended during the turn. Tilt and accelerometer errors, which had become correlated in the straight and level portion of the flight, were probably being decorrelated by the turn. When the alignment ended, these decorrelated errors had not yet been estimated out. To test this hypothesis and demonstrate

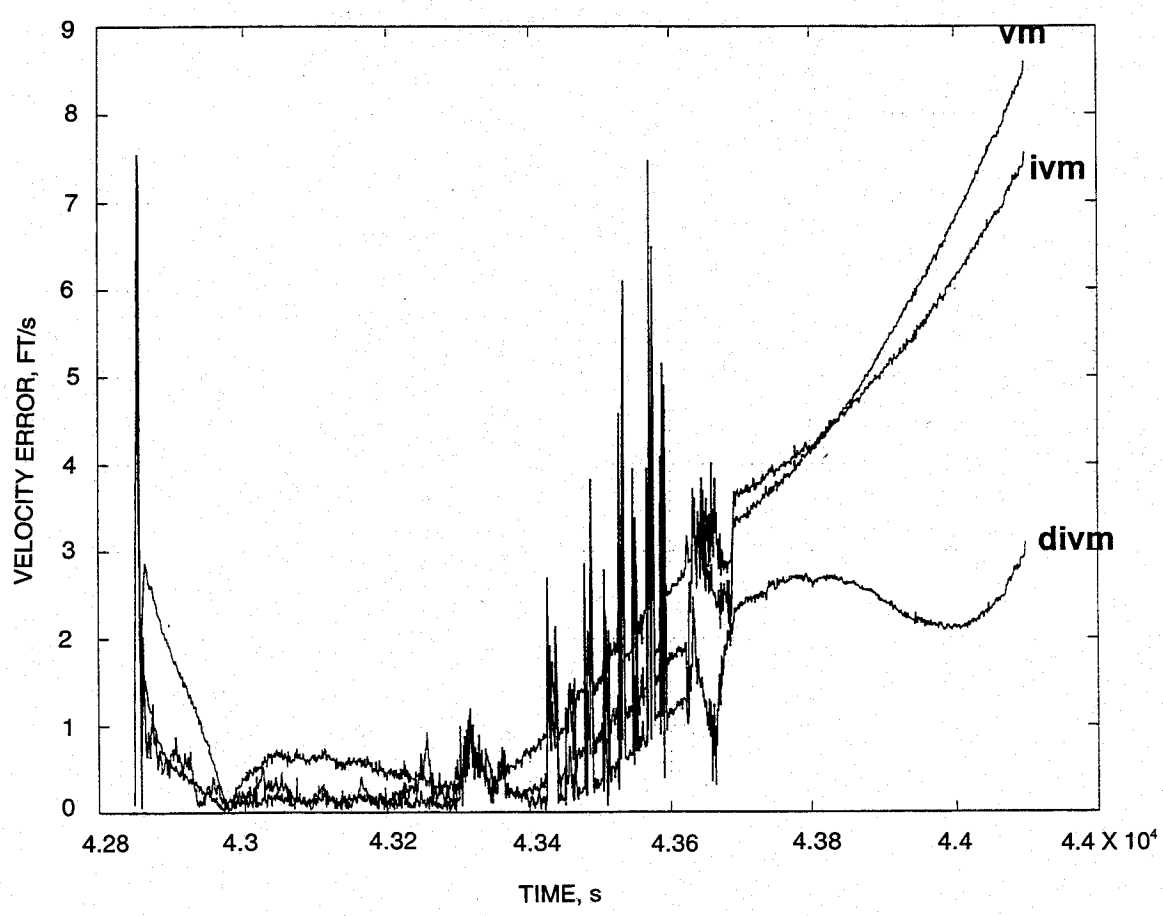

FIGURE 9. Velocity Error Versus Time (60-Degree Turn).

the ability to mix alignment modes, we added gyro-based measurements to the velocity matching alignment during the turn. Everything else remains the same. The results are shown in Figure 10. The velocity matching alignment from Figure 9 is included as a reference. We observe a significant improvement in alignment quality for any of the combination alignments over velocity matching alone.

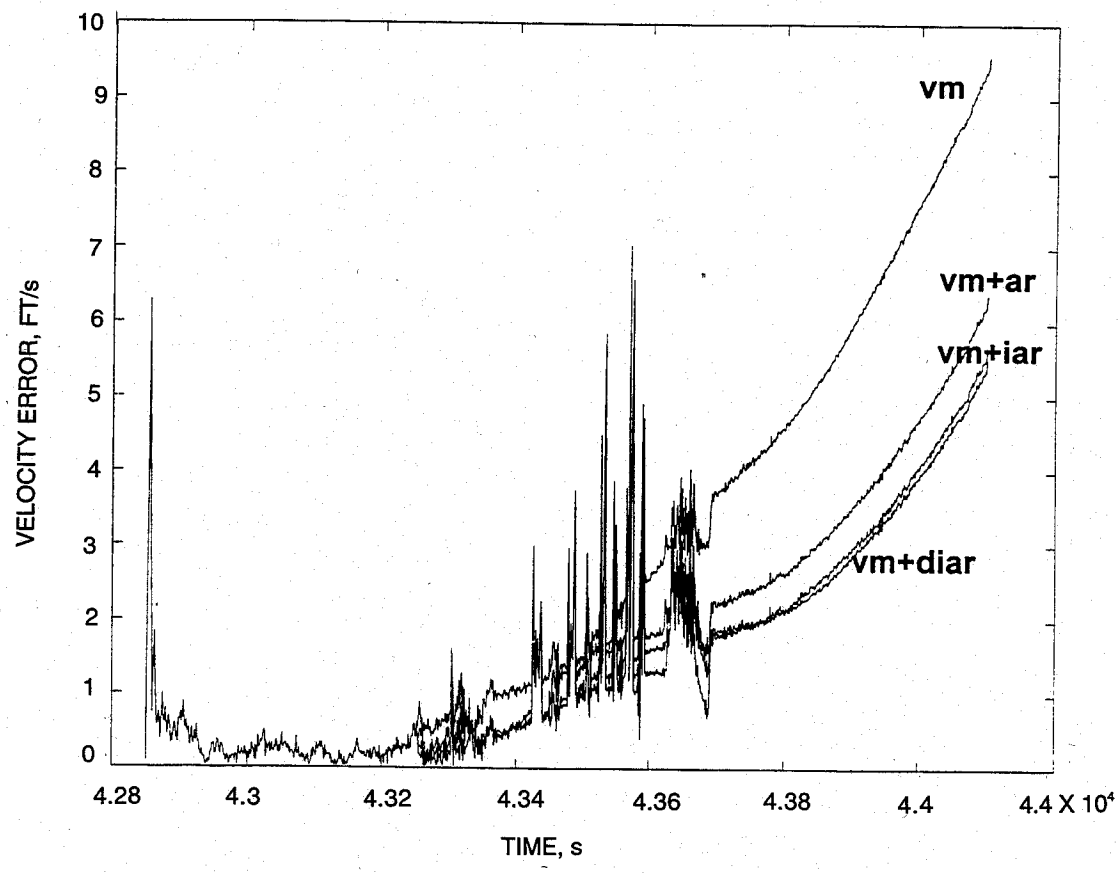

FIGURE 10. Velocity Error Versus Time With Gyro-Based Measurements Added.

Finally, we present plots of the differences between the slave and master pitch and roll for integrated angular rate alignments (Figures 11 and 12). The alignment time extends through the series of turns. Because the slave is mechanically misaligned from the master, we do not know the "true" tilts. All we can observe is that the delta pitch and delta roll angles at the end of the alignment are consistent with many alignments performed on this data. Incidentally, the delta pitch, roll, and heading angles are functions of the attitude of the aircraft; the best we can do is compare the values for straight and level flight.

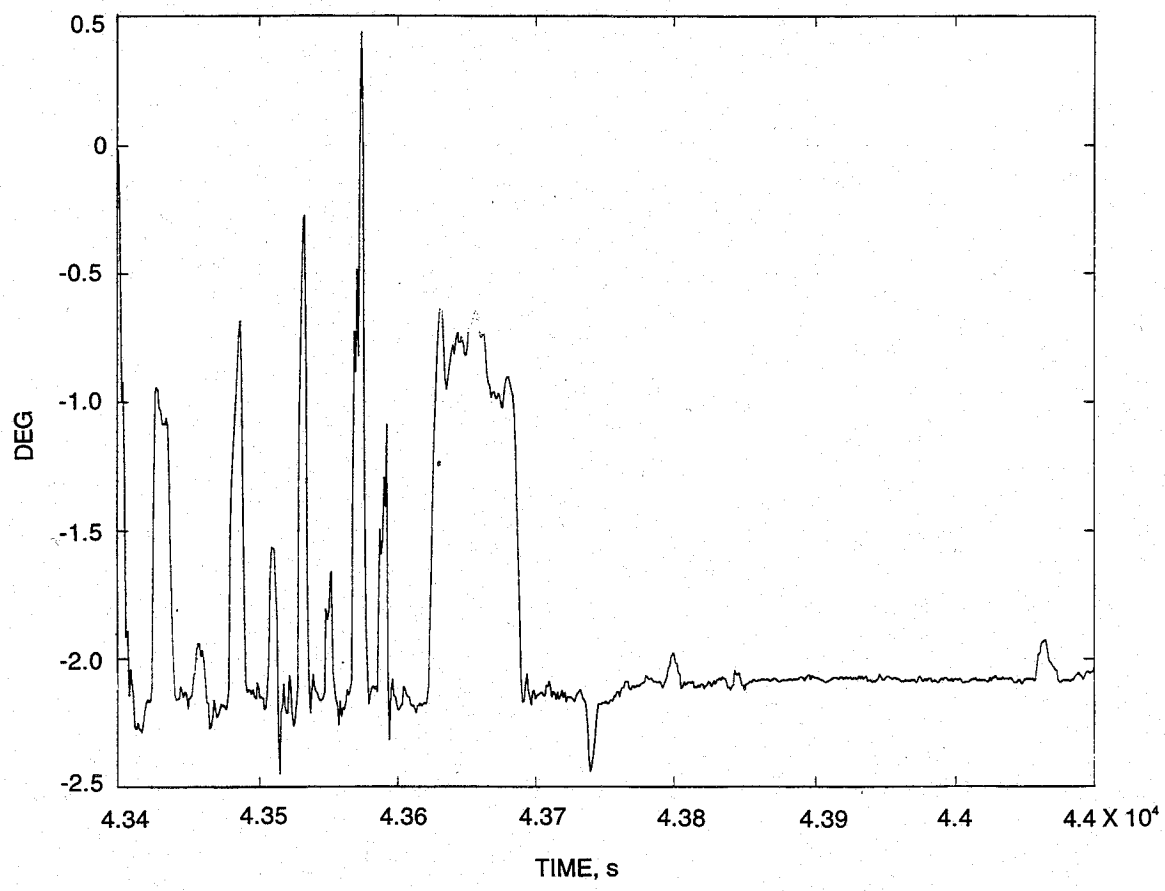

FIGURE 11. Delta Pitch.

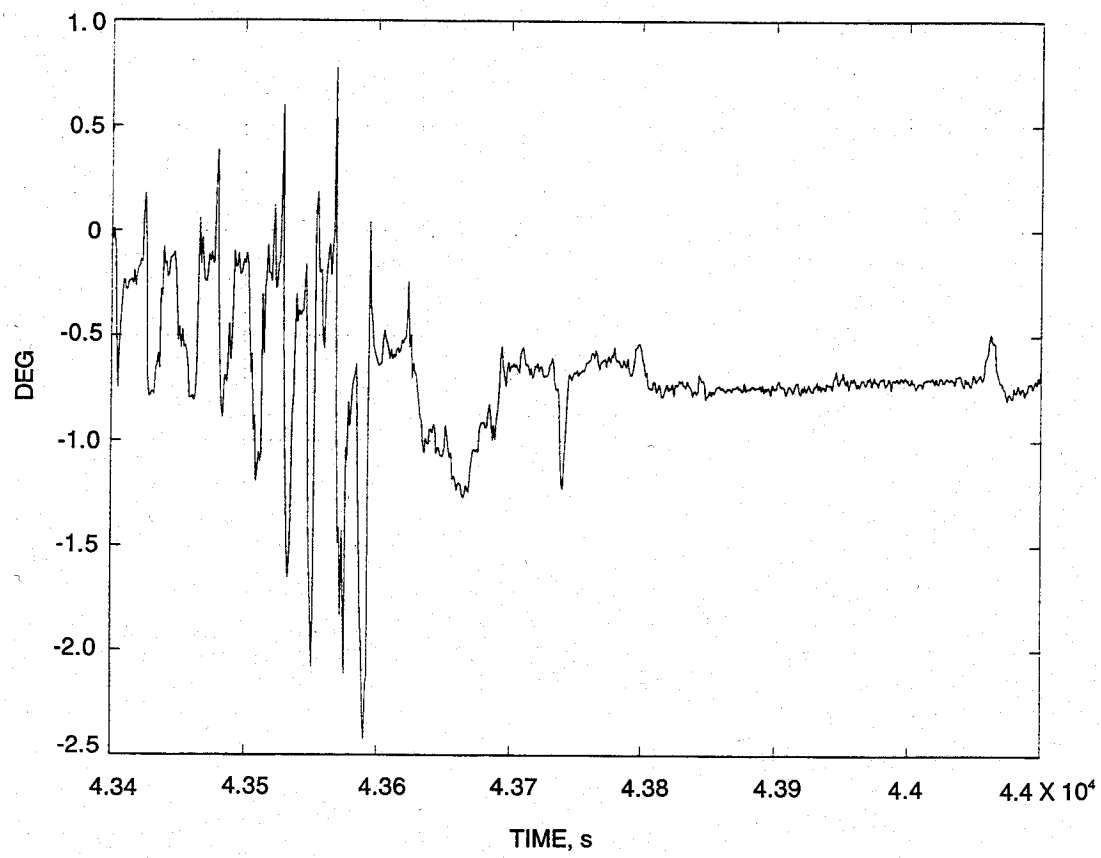

FIGURE 12. Delta Roll.

SUMMARY

We have not presented an exhaustive analysis of any of the alignment mechanizations in this report. We have tried to indicate what some of the more common alignment methods are and some of the advantages and disadvantages of each. Every system has its own unique problems, and no single alignment method is best for all. An analysis needs to be performed to determine the appropriate method in each case. We have also tried to indicate some of the tools available for transfer alignment analysis.

In the Appendix we have presented detailed derivations for each of the alignment algorithms discussed. We emphasize that these derivations are not unique; there are many ways to formulate the measurement for each type of alignment.

Page Left Blank

Appendix
MEASUREMENT EQUATIONS

ACCELEROMETER-BASED ALIGNMENTS

Velocity Matching

Velocity matching is the most common type of alignment. The measurement consists of a comparison of the master and slave navigation velocities. We will derive the measurement equations for a three-axis alignment, although sometimes the vertical velocity is not used because the vertical channel is controlled by a baro-inertial loop in most aircraft applications. The inertial data in the vertical reference channel are thus corrupted by resets from the baro loop.

It is assumed that the master and slave are separated by a moment arm (fixed in the body axes), $\mathbf{r}$. Let $\mathbf{R}_m$ and $\mathbf{R}_s$ be the position vectors of the master and slave, respectively. In Earth Centered Earth Fixed (ECEF) coordinates

$$\mathbf{R}_s^E = \mathbf{R}_m^E + \mathbf{r}^E. \tag{1}$$

By definition, $\mathbf{V}^E = \dot{\mathbf{R}}^E$ *so* $\mathbf{V}_s^E = \mathbf{V}_m^E + \dot{\mathbf{r}}^E$. Transforming to some local level frame, L,

$$\mathbf{V}_s^L = \mathbf{V}_m^L + C_E^L \dot{\mathbf{r}}^E. \tag{2}$$

From $\mathbf{r}^E = C_B^E \mathbf{r}^B$ and $\dot{\mathbf{r}}^B = 0$, we have

$$\dot{\mathbf{r}}^E = \dot{C}_B^E \mathbf{r}^B. \tag{3}$$

Substituting Equation 3 into Equation 2, we have $\mathbf{V}_s^L = \mathbf{V}_m^L + C_E^L \dot{C}_B^E \mathbf{r}^B$. This can be written as

$$\mathbf{V}_s^L = \mathbf{V}_m^L - \Omega_{EB}^L C_B^L \mathbf{r}^B \tag{4}$$

where

$$\Omega \equiv \begin{bmatrix} 0 & \omega_3 & -\omega_2 \\ -\omega_3 & 0 & \omega_1 \\ \omega_2 & -\omega_1 & 0 \end{bmatrix}$$

and $\boldsymbol{\omega}_{EB}^{L}$ is the angular rate of the body frame with respect to the ECEF frame in local level coordinates.

The master and the slave do not necessarily navigate in the same frame. We assume here that the master always navigates in the North-East-Down (NED) frame and the slave in a wander azimuth frame (L-frame). Let C_L^N be the transformation from wander azimuth to NED

$$C_L^N = \begin{bmatrix} \cos\alpha & -\sin\alpha & 0 \\ \sin\alpha & \cos\alpha & 0 \\ 0 & 0 & 1 \end{bmatrix}.$$

We rewrite Equation 4 as

$$C_L^N \mathbf{V}_s^L = \mathbf{V}_m^N - \Omega_{EB}^N C_B^N \mathbf{r}^B = \mathbf{V}_m^N + \boldsymbol{\omega}_{EB}^N \times \mathbf{r}^N. \tag{5}$$

The $\boldsymbol{\omega}_{EB}^N \times \mathbf{r}^N$ terms could be computed by either the master or slave. If the moment arms are accurately known, the more accurate solution is to compute these terms in the master, because the slave senses vibration and flexure in its measured angular rates. This flexure crossed with the moment arms produces noise on the measurements. The effect can be severe for high levels of vibration (see References 3 and 4). In many cases, however, it is impractical to compute these terms in the master. Another advantage of computing these terms in the slave is that if the moment arms are not accurately known, they can be estimated by the slave's filter. The velocity-based alignments are mechanized both ways in the simulation. In this appendix we assume that these terms are computed by the master.

In terms of quantities computed by the master INS model we have

$$\boldsymbol{\omega}_{EB}^N \times \mathbf{r}^N = (\boldsymbol{\omega}_{IB}^N - \boldsymbol{\omega}_{IE}^N) \times \mathbf{r}^N \tag{6}$$

where $\boldsymbol{\omega}_{IB}^N = C_B^N \boldsymbol{\omega}_{IB}^B$ is body rate, $\boldsymbol{\omega}_{IE}^N = C_E^N \boldsymbol{\omega}_{IE}^E$ is Earth rate, and $\mathbf{r}^N = C_B^N \mathbf{r}^B$. We define the velocity measurement from the master as

$$\tilde{\mathbf{V}} = \mathbf{V}_m^N + (\boldsymbol{\omega}_{IB}^N - \boldsymbol{\omega}_{IE}^N) \times \mathbf{r}^N, \tag{7}$$

then our measurement takes the form

$$\mathbf{Z} = \hat{C}_L^N \hat{\mathbf{V}}_S^L - \tilde{\mathbf{V}} + \boldsymbol{\eta}. \tag{8}$$

where a circumflex indicates an estimated quantity and a tilde indicates a measured value.

The quantity $\tilde{\mathbf{V}}$ is the velocity of a rigid body displaced from the master INS by $\mathbf{r}$. The velocity sensed by the slave differs from $\tilde{\mathbf{V}}$ by the linear vibration and flexure of the slave with respect to the master. For no system or sensor errors we would have

$$\mathbf{V}_s \equiv \tilde{\mathbf{V}} + \Delta\mathbf{V}.$$

In terms of the error states

$$\hat{\mathbf{V}}_s^L \equiv \mathbf{V}_s^L + \delta\mathbf{V}_s^L$$

and

$$\hat{C}_L^N \equiv C_L^N + \delta C_L^N$$

where

$$\delta C_L^N = C_L^N \begin{bmatrix} 0 & -\delta\alpha & 0 \\ \delta\alpha & 0 & 0 \\ 0 & 0 & 0 \end{bmatrix} = \begin{bmatrix} 0 & -\delta\alpha & 0 \\ \delta\alpha & 0 & 0 \\ 0 & 0 & 0 \end{bmatrix} C_L^N.$$

Substituting these relations into Equation 8, we obtain

$$\mathbf{Z} = (C_L^N + \delta C_L^N)(\mathbf{V}_S^L + \delta\mathbf{V}_S^L) - \tilde{\mathbf{V}} + \boldsymbol{\eta}$$

or

$$\mathbf{Z} = C_L^N \delta \mathbf{V}_S^L - (C_L^N \mathbf{V}_S^L) \times \delta\boldsymbol{\alpha} + \Delta \mathbf{V}^N + \boldsymbol{\eta} \tag{9}$$

where

$$\delta\boldsymbol{\alpha} = \begin{pmatrix} 0 \\ 0 \\ \delta\alpha \end{pmatrix}$$

and η is a noise vector.

We can model the $\Delta\mathbf{V}$ terms as states. This requires adding six states to the filter to model linear vibration. For k=x,y,z these are $\dot{\xi}_k, \xi_k$, which are defined to be the velocity and displacement of the linear vibration in the slave's body frame. In terms of these states Equation 9 becomes

$$\mathbf{Z} = C_L^N \delta \mathbf{V}_S^L - (C_L^N \mathbf{V}_S^L) \times \delta\boldsymbol{\alpha} + C_B^N \dot{\boldsymbol{\xi}} + \boldsymbol{\eta}. \tag{10}$$

These states are to be treated as consider variables by the filter. The gains for these states must be zeroed after the gains computation. The F-matrix elements are defined by the equations

$$d/dt \begin{pmatrix} \dot{\xi} \\ \xi \end{pmatrix}_k = \begin{bmatrix} -2\alpha_k\beta_k & -\beta_k^2 \\ 1 & 0 \end{bmatrix} \begin{pmatrix} \dot{\xi} \\ \xi \end{pmatrix}_k + \begin{pmatrix} Nv_k \\ 0 \end{pmatrix} \tag{11}$$

for $k = x,y,z$ and Nv_k = power spectral density of the white noise process. Equations 11 are the state vector form of a second order Markov process of the form

$$\ddot{\mu} + 2\alpha\beta\dot{\mu} + \beta^2\mu = W.$$

Depending on the choice of α and β and the integration rate for the State Transition Matrix (STM), Equations 11 may not converge. A stable method is to zero the F-matrix elements for the flexure states and compute the STM as usual, then set the diagonal elements of the STM for these states to zero. Before performing the time update, compute the STM elements for these states by the method outlined below. Assume $\alpha < 1$ and define

$$\omega = \sqrt{1 - \alpha^2}$$

$$A_1 = e^{-\alpha\beta\Delta t}\cos\omega\beta\Delta t,$$

and

$$A_2 = \frac{1}{\omega}e^{-\alpha\beta\Delta t}\sin\omega\beta\Delta t.$$

Then

$$\dot{x}_{p+1} = (A_1 - \alpha A_2)\dot{x}_p - \beta A_2 x_p + v_{p+1} \tag{12}$$

and

$$x_{p+1} = \frac{1}{\beta}A_2\dot{x}_p + (A_1 + \alpha A_2)x_p + u_{p+1}$$

where v_{p+1} and u_{p+1} are discrete sequences computed from the defining white noise process. These will appear as process noise terms in the filter. They may be computed as follows.

$$\sigma_v^2 = \frac{N}{4\alpha\beta\omega^2}\left[\omega^2 + e^{-2\alpha\beta\Delta t}\left(\alpha^2\cos 2\beta\omega\Delta t + \alpha\omega\sin 2\beta\omega\Delta t - 1\right)\right] \tag{13}$$

$$\sigma_u^2 = \frac{N}{4\alpha\beta^3\omega^2}\left[\omega^2 + e^{-2\alpha\beta\Delta t}\left(\alpha^2\cos 2\beta\omega\Delta t - \alpha\omega\sin 2\beta\omega\Delta t - 1\right)\right]$$

where N is the power spectral density of the white noise driving the process. Then $Q_v^2 = \sigma_v^2\Delta t$ and $Q_u^2 = \sigma_u^2\Delta t$. In our formalism, Equations 12 become

$$\begin{pmatrix} \dot{x}(t+\Delta t) \\ x(t+\Delta t) \end{pmatrix} = \begin{pmatrix} A_1 - \alpha A_2 & -\beta A_2 \\ \frac{1}{\beta}A_2 & A_1 + \alpha A_2 \end{pmatrix}\begin{pmatrix} \dot{x}(t) \\ x(t) \end{pmatrix} + \begin{pmatrix} Q_v \\ Q_u \end{pmatrix}. \tag{14}$$

Typical values for the parameters in Equation 13 are $N_v = 0.4\ ft^2/s^3$, a = 0.4, b = 20/s. For these values, the steady state variance of $\dot{\xi}$ is

$$\sigma_v^2 = \frac{N_v}{4\alpha\beta} = (0.11 ft/\sec)^2$$

and for ξ is

$$\sigma_u^2 = \frac{N_v}{4\alpha\beta^3} = (0.0056ft)^2$$

The generalization of these equations for $\alpha \geq 1$ is straightforward. A simpler and fairly effective method of modeling the vibration noise and flexure is to approximate it in the filter as white noise. In a velocity matching alignment it would appear as measurement noise. Thus in Equation 9 the effective measurement noise would be $\boldsymbol{\eta}' = \Delta \mathbf{V}^N + \boldsymbol{\eta}$. Equation 9 would then take the form

$$\mathbf{Z} = C_L^N \delta \mathbf{V}_S^L - (C_L^N \mathbf{V}_S^L) \times \delta\boldsymbol{\alpha} + \boldsymbol{\eta}'. \tag{15}$$

In an integrated or doubly integrated velocity matching alignment it would appear as process noise on the velocity integral states.

Integrated Velocity Matching

The measurement takes the form of the integral of Equation 8

$$\mathbf{Z} = \int_{t_o}^{t} \left[\hat{C}_L^N \hat{\mathbf{V}}_S^L - \tilde{\mathbf{V}} + \boldsymbol{\eta}\right] d\tau. \tag{16}$$

A digression is at this point to clearly explain the role the noise terms play in the integrated measurements. Let us assume that we have a scalar measurement consisting of the difference in the value of some quantity, ρ, computed in the master and slave frames. Thus

$$z_o = \rho_s - \rho_m + \eta \tag{17}$$

where as usual η is a noise term. We define the first and second integrals of this measurement as

$$z_1 = \int \left[\rho_s - \rho_m + \eta\right] d\tau \tag{18}$$

and

$$z_2 = \int\int [\rho_s - \rho_m + \eta]\, d\lambda d\tau. \tag{19}$$

If we define

$$\delta p = \int [\rho_s - \rho_m]\, d\tau \tag{20}$$

then

$$z_1 = \delta p + \int \eta d\tau = \delta p + \eta' \tag{21}$$

and

$$\frac{d}{dt}\delta p = \rho_s - \rho_m. \tag{22}$$

For the second integral

$$\delta pp = \int\int [\rho_s - \rho_m]\, d\lambda d\tau \tag{23}$$

which gives

$$z_2 = \delta pp + \int\int \eta d\lambda d\tau = \delta pp + \eta'' \tag{24}$$

and

$$\frac{d}{dt}\delta pp = \delta p. \tag{25}$$

If η is a white noise term, the noise terms η' and η'' in Equations 21 and 24 are certainly not. This violates the definition of measurement noise in the Kalman filter. We do note that the variance associated with η'' will be less than the variance of η'. From Equations 22 and 25 we see that the states δp and δpp are not driven by any process noise.

If, on the other hand, we define

$$\delta p = z_1 = \int [\rho_s - \rho_m + \eta]\, d\tau, \tag{26}$$

then Equations 21 and 22 become

$$z_1 = \delta p \tag{27}$$

and

$$\frac{d}{dt}\delta p = \rho_s - \rho_m + \eta. \tag{28}$$

Now there is no noise on the measurement and the state δp is driven by a white noise term that is modeled as process noise in the filter. The second integral is modeled as

$$\delta pp = \int\int [\rho_s - \rho_m + \eta]\, d\lambda d\tau \tag{29}$$

which gives

$$z_2 = \delta pp \tag{30}$$

and

$$\frac{d}{dt}\delta pp = \delta p. \tag{31}$$

There is no noise on the z_2 measurement and no process noise on the δpp states. Thus by the definition of Equations 26 and 29 we have avoided violating the conditions on the Kalman filter. There is one problem with the definitions of Equations 26 and 29. Since there is no measurement noise associated with z_1, the second integration does nothing to reduce the effective noise; the alignment will be equivalent for both cases. This analysis is confirmed by simulation results. Whether the second integral reduces alignment time or required alignment maneuvers was not investigated. The correct solution is to add the necessary states to model η'' and η' as states driven by white noise. Alternatively, we could use Equation 26 to define the first integrals and Equation 24 to define the second integrals.

In constructing the measurement for integrated velocity matching we assume that Equation 7 is computed by the master and sent to the slave at a high rate ($\geq$ 50 Hz) or that the master computes $\int_{t_o}^{t} \tilde{\mathbf{V}} d\tau$ and sends it to the slave at the measurement rate. The

expansion of Equation 16 in terms of error states is given by the integral of Equation 9 or 10. If we use Equation 9 we have

$$\mathbf{Z} = \int_{t_0}^{t} \left[C_L^N \delta \mathbf{V}_S^L - (C_L^N \mathbf{V}_S^L) \times \delta \boldsymbol{\alpha} + \boldsymbol{\eta}' \right] d\tau, \tag{32}$$

or if we use (10) we have

$$\mathbf{Z} = \int_{t_0}^{t} \left[C_L^N \delta \mathbf{V}_S^L - (C_L^N \mathbf{V}_S^L) \times \delta \boldsymbol{\alpha} + C_B^N \dot{\boldsymbol{\xi}} + \boldsymbol{\eta} \right] d\tau. \tag{33}$$

In either case we define a new set of states as

$$\delta \mathbf{P} = \mathbf{Z}. \tag{34}$$

The measurement matrix is now trivial; it just consists of ones for these states. The F-matrix elements for these states are given by

$$\delta \dot{\mathbf{P}} = C_L^N \delta \mathbf{V}_S^L - (C_L^N \mathbf{V}_S^L) \times \delta \boldsymbol{\alpha} + \boldsymbol{\eta}' \tag{35}$$

or

$$\delta \dot{\mathbf{P}} = C_L^N \delta \mathbf{V}_S^L - (C_L^N \mathbf{V}_S^L) \times \delta \boldsymbol{\alpha} + C_B^N \dot{\boldsymbol{\xi}} + \boldsymbol{\eta}. \tag{36}$$

Note that we have defined $\boldsymbol{\eta}' = \Delta \mathbf{V}^{\mathrm{N}} + \boldsymbol{\eta}$ as the effective noise when we do not model the flexure states. The simulation mechanizes both Equations 32 and 33. We do not add states for the $\boldsymbol{\eta}$ terms as they are much smaller than the $\Delta \mathbf{V}$ terms. In either case the measurement noise for the velocity matching states appears as process noise for the velocity integral states. There is no theoretical measurement noise for the velocity integral measurements (neglecting computational error). The measurement noise for this type of alignment should be set to some small, nonzero value.

Doubly Integrated Velocity Matching

The measurement takes the form of the double integral of Equation 8

$$\mathbf{Z} = \int_{t_o}^{t} \int_{t_0}^{\tau} \left[\hat{C}_L^N \hat{\mathbf{V}}_S^L - \tilde{\mathbf{V}} + \boldsymbol{\eta} \right] d\lambda d\tau. \tag{37}$$

Expanding these states as before

$$\mathbf{Z} = \int_{t_0}^{t} \int_{t_0}^{\tau} \left[C_L^N \delta \mathbf{V}_S^L - (C_L^N \mathbf{V}_S^L) \times \delta \boldsymbol{\alpha} + \boldsymbol{\eta}' \right] d\lambda d\tau \tag{38}$$

or, if we model flexure and vibration as states,

$$\mathbf{Z} = \int_{t_0}^{t} \int_{t_0}^{\tau} \left[C_L^N \delta \mathbf{V}_S^L - (C_L^N \mathbf{V}_S^L) \times \delta \boldsymbol{\alpha} + C_B^N \dot{\boldsymbol{\xi}} + \boldsymbol{\eta} \right] d\lambda d\tau. \tag{39}$$

These two equations can be combined as

$$\mathbf{Z} = \int_{t_0}^{t} \delta \mathbf{P} d\tau. \tag{40}$$

We assume that the velocity integral states have been previously defined as in Equation 34. We now define three more states as

$$\delta \mathbf{PP} = \mathbf{Z}. \tag{41}$$

The measurement matrix is again trivial, consisting of ones on these states. The F-matrix elements are found from

$$\frac{d}{dt} \delta \mathbf{PP} = \int_{t_0}^{\tau} \left[\hat{C}_L^N \hat{\mathbf{V}}_S^L - \tilde{\mathbf{V}} + \boldsymbol{\eta} \right] d\lambda = \delta \mathbf{P}. \tag{42}$$

There is no theoretical process noise associated with $\delta \mathbf{PP}$ and no measurement noise with Equation 37.

GYRO-BASED ALIGNMENTS

Angular Rate Matching

A gyro measures the angular rate about its input axes with respect to inertial space. A set of three gyros in an orthogonal configuration defines a set of body axes. The gyros then measure the angular rate of these body axes with respect to inertial space, $\boldsymbol{\omega}_{IB}^{B}$, in body axes. For transfer alignment purposes, we assume that the master INS measures the true angular rate. We also assume that, except for flexure and vibration, the body axes of the master and slave are fixed with respect to each other.

To compare the angular rates as measured by the master and the slave, we transform to a local level frame with a body to local transformation, C_B^L. Let

I = inertial frame,
B = slave's body frame
B′= master's body frame
L = local frame

and

$\omega_{B'B}$ = angular rate due to flexure and vibration.

Our measurement is

$$\mathbf{Z} = \hat{C}_B^L \tilde{\omega}_{IB}^B - C_{B'}^L \omega_{IB'}^{B'} + \eta \tag{43}$$

where

$\omega_{IB'}^{B'}$ = master's measurement of its body rate
$C_{B'}^L$ = master's estimate of its body to local level transformation
$\tilde{\omega}_{IB}^B$ = slave's measurement of its body rate
$\hat{C}_B^L$ = slave's estimate of its body to local level transformation

and

η = noise.

Both $\tilde{\omega}_{IB}^B$ and $\hat{C}_B^L$ will contain errors; $\tilde{\omega}_{IB}^B = \omega_{IB}^B + \delta\omega_{IB}^B$ and $\hat{C}_B^L = C_B^L + \delta C_B^L$. When we substitute these into Equation 43

$$\mathbf{Z} = C_B^L \omega_{IB}^B - C_{B'}^L \omega_{IB'}^{B'} + \delta C_B^L \omega_{IB}^B + C_B^L \delta\omega_{IB}^B + \eta. \tag{44}$$

Using $\omega_{IB} = \omega_{IB'} + \omega_{B'B}$, we have

$$C_B^L \omega_{IB}^B - C_{B'}^L \omega_{IB'}^{B'} = C_B^L \omega_{IB'}^B + C_B^L \omega_{B'B}^B - C_{B'}^L \omega_{IB'}^{B'} = C_B^L \omega_{B'B}^B. \tag{45}$$

Substituting this back into our measurement

$$\mathbf{Z} = C_B^L \boldsymbol{\omega}_{B'B}^B + \delta C_B^L \boldsymbol{\omega}_{IB}^B + C_B^L \delta \boldsymbol{\omega}_{IB}^B + \boldsymbol{\eta}. \tag{46}$$

We make the substitution $\delta C_B^L = -C_B^L(\psi)$ where ψ is the misalignment error in body coordinates and

$$(\psi) = \begin{bmatrix} 0 & \psi_z & -\psi_y \\ -\psi_z & 0 & \psi_x \\ \psi_y & -\psi_x & 0 \end{bmatrix}. \tag{47}$$

To simplify the notation we define $\boldsymbol{\omega}_{B'B}^B = \Delta\boldsymbol{\omega}$, $\boldsymbol{\omega}_{IB}^B = \boldsymbol{\omega}$, and $C_B^L = C$. Our measurement equation becomes

$$\mathbf{Z} = -(C\boldsymbol{\omega}) \times \boldsymbol{\psi}^L + C\delta\boldsymbol{\omega} + C\Delta\boldsymbol{\omega} + \boldsymbol{\eta}. \tag{48}$$

The first term on the right is expressed in terms of the usual tilt and heading errors. The second term contains the gyro errors. The angular flexure and vibration terms, $\Delta\boldsymbol{\omega}$, are handled in exactly the same way as the linear flexure and vibration terms, $\Delta\mathbf{V}$, were treated in the accelerometer-based alignments.

If the master rotates its body rates to the NED frame before transmitting them to the slave, Equation 43 becomes

$$\mathbf{Z}' = \hat{C}_B^L \tilde{\boldsymbol{\omega}}_{IB}^B - \hat{C}_N^L C_{B'}^N \boldsymbol{\omega}_{IB'}^{B'} + \boldsymbol{\eta}. \tag{49}$$

This gives us an additional term in Equation 46, because

$$\mathbf{Z}' = \mathbf{Z} - \delta C_N^L C_{B'}^N \boldsymbol{\omega}_{IB'}^{B'}.$$

In terms of Equation 48 we have

$$\delta C_N^L C_{B'}^N \boldsymbol{\omega}_{IB'}^{B'} = \begin{bmatrix} 0 & \delta\alpha & 0 \\ -\delta\alpha & 0 & 0 \\ 0 & 0 & 0 \end{bmatrix} C_{B'}^L \boldsymbol{\omega}_{IB'}^{B'} \simeq \begin{bmatrix} 0 & \delta\alpha & 0 \\ -\delta\alpha & 0 & 0 \\ 0 & 0 & 0 \end{bmatrix} C\boldsymbol{\omega} = -\delta\boldsymbol{\alpha} \times C\boldsymbol{\omega}$$

where

$$\delta\boldsymbol{\alpha} = \begin{pmatrix} 0 \\ 0 \\ \delta\alpha \end{pmatrix}.$$

Equation 48 becomes

$$\mathbf{Z}' = \mathbf{Z} - C\boldsymbol{\omega} \times \delta\boldsymbol{\alpha}. \tag{50}$$

Note that the form of the H-matrix depends on how we model the flexure and whether we must rotate the angular rate from the master.

Integrated Angular Rate Matching

For the measurement of integrated angular rate matching, we integrate the gyro output in the navigation frame. This is simpler than (but equivalent to) attitude matching, as we do not need to know how the Euler angles are defined in the master and slave. The measurement is defined as the integral of Equation 43:

$$\mathbf{Z} = \int_{t_0}^{t} \left[\hat{C}_B^L \tilde{\boldsymbol{\omega}}_{IB}^B - C_{B'}^L \boldsymbol{\omega}_{IB'}^{B'} + \boldsymbol{\eta} \right] d\tau. \tag{51}$$

We can expand Equation 51 as in the previous section to obtain

$$\mathbf{Z} = \int_{t_0}^{t} \left[-(C\boldsymbol{\omega}) \times \boldsymbol{\psi}^L + C\delta\boldsymbol{\omega} + C\Delta\boldsymbol{\omega} + \boldsymbol{\eta} \right] d\tau. \tag{52}$$

We define three new states for this measurement as

$$\delta\mathbf{A} = \mathbf{Z}. \tag{53}$$

The observation matrix is now trivial, consisting of ones on the $\delta\mathbf{A}$ states. The F-matrix elements are found from

$$\delta\dot{\mathbf{A}} = -\left(C\boldsymbol{\omega}\right) \times \boldsymbol{\psi}^L + C\delta\boldsymbol{\omega} + C\Delta\boldsymbol{\omega} + \boldsymbol{\eta}. \tag{54}$$

In the case where we do not model the flexure as states, the effective process noise on the $\delta\mathbf{A}$ states is $\boldsymbol{\eta}' = \int_{t_0}^{t} C\Delta\boldsymbol{\omega} d\tau + \boldsymbol{\eta}$. For the case where we model the $\Delta\boldsymbol{\omega}$ terms as states, the

process noise is just $\boldsymbol{\eta}$. The observation matrix is unchanged. The F-matrix contains additional terms due to flexure,

$$\delta\dot{\mathbf{A}}' = \delta\dot{\mathbf{A}} + C \begin{pmatrix} \dot{\mu}_x \\ \dot{\mu}_y \\ \dot{\mu}_z \end{pmatrix} \tag{55}$$

where $\dot{\mu}$ are the angular equivalent of the $\dot{\boldsymbol{\xi}}$ states defined in Equation 11.

For the case where the master navigates in NED and the slave in wander azimuth, the measurement must be computed as

$$\mathbf{Z}' = \int_{t_0}^{t} \left[\hat{C}_B^L \tilde{\boldsymbol{\omega}}_{IB}^B - C_N^L C_{B'}^N \boldsymbol{\omega}_{IB'}^{B'} + \boldsymbol{\eta}\right] d\tau = \mathbf{Z} - \begin{bmatrix} 0 & \delta\alpha & 0 \\ -\delta\alpha & 0 & 0 \\ 0 & 0 & 0 \end{bmatrix} \int_{t_0}^{t} C\boldsymbol{\omega} d\tau.$$

The measurement matrix does not change. The only correction is the addition of the term

$$-(C\boldsymbol{\omega}) \times \boldsymbol{\alpha} \tag{56}$$

to the right-hand side of Equation 54.

Doubly Integrated Angular Rate Matching

The measurement for doubly integrated angular rate matching is defined as

$$\mathbf{Z} = \int_{t_0}^{t} \int_{t_0}^{\tau} \left[\hat{C}_B^L \tilde{\boldsymbol{\omega}}_{IB}^B - C_{B'}^L \boldsymbol{\omega}_{IB'}^{B'} + \boldsymbol{\eta}\right] d\lambda d\tau. \tag{57}$$

As before, we define three new states

$$\delta\mathbf{AA} = \mathbf{Z} \tag{58}$$

The observation matrix is again trivial. The new F-matrix elements are found from

$$\frac{d}{dt}\delta\mathbf{AA} = \delta\mathbf{A}. \tag{59}$$

There is no process noise associated with these states.

REFERENCES

1. U.S. Air Force. *Advanced Alignment Concepts*, by Jim Kain, The Analytic Sciences Corporation; Reading, Mass. October 1989. (AFATL-TR-89-50.)

2. William R. Graham and Kevin J. Shortelle, System Dynamics International, Gainsville, Fla. "Advanced Transfer Alignment for Inertial Navigators," *in ION National Technical Meeting Proceedings*, January 1995.

3. Robert M. Rogers, Rogers Engineering & Associates, Gainsville, Fla. "Velocity-Plus-Rate Matchiong for Improved Tactical Weapon Rapid Transfer Alignment," presented at AIAA conference, 1996.

4. Naval Weapons Center. *Transfer Alignment Methods Study for Air Launched Missiles*, by Paul G. Savage and D. Brent Miller, Strapdown Associates, Inc., Plymouth, Minn. China Lake, Calif., NWC, April 1990. (NWC-005-005.)

5. _____. *Transfer Alignment Applications Study for Air Launched Missiles*, by Paul G. Savage and D. Brent Miller, Strapdown Associates, Inc., Plymouth, Minn. China Lake, Calif., NWC, October 1990. (NWC-007-003.)

6. Naval Air Warfare Center Weapons Division. *Effect of Angular Vibration on Transfer Alignment*, by S. H. Stovall. China Lake, Calif., NAWCWPNS, June 1993.

7. _____. *Effect of Angular Vibration on Transfer Alignment II*, by S. H. Stovall. China Lake, Calif., NAWCWPNS, January 1994.